CHARACTERIZATION OF VECTOR FIELDS BASED ON AN ANALYSIS OF THEIR LOCAL EXPANSIONS

ANDRÉ BUCHAU & JENS ANDERS
Institute of Smart Sensors, University of Stuttgart, Germany

ABSTRACT

The goal of the presented study is to provide a systematic approach for the efficient characterization of vector fields inside a defined region of interest. That means the vector field is described there with a set of coefficients that can be easily derived from the field values and that contains enough information to characterize the vector field accurately. A possible field of application of this approach is the design of defined distributions of vector fields for specific use cases based on optimization algorithms or machine learning approaches. For instance, the homogeneity of the magnetic B-field is an important measure in the context of nuclear magnetic resonance spectroscopy since it directly limits the achievable spectral resolution and applicability of this method. Here, we present a new combination of established techniques of modern boundary element methods, which are typically used for the solution of the field problem, with automatic analysis of the so-called local expansion of the fast multipole method to characterize a vector field based on a robust approach. The local expansion represents the field inside a defined domain, and the effect of all field sources outside this domain is replaced by a small set of local coefficients. Hence, we first discuss the meaning of these local coefficients and then show how they can be computed directly by a smart use of Green's theorem. Finally, we show the spectrum of local coefficients, which, in the next step, is the basis for a cost function of an optimization problem of the studied vector field.

Keywords: Laplace's equation, boundary element method, fast multipole method, homogeneous fields, spherical harmonics, vector field characterization.

1 INTRODUCTION

The characterization of a vector field is a challenging task, even in the stationary case. A common approach is to visualize the studied vector field and extract information about the field distribution for further optimization. A typical example is shown in Fig. 1 where the B-field of a magnet is plotted. The depicted B-field in the region of interest (ROI) appears homogeneous. However, a characterization only based on visualization is not measurable and not algorithmically useable. Hence, the goal is to find parameters for the characterization of the vector field, which are easy to compute and contain enough information about the field to enable computer-based processing of the results.

Such a parameter is the homogeneity value of a single component V_z of the vector field $\boldsymbol{V}$

$$\eta = \frac{\max(V_z) - \min(V_z)}{\int_{\Omega_{\mathrm{ROI}}} V_z \mathrm{d}V} \Omega_{\mathrm{ROI}}, \tag{1}$$

where Ω_{ROI} is the domain of the ROI. The homogeneity value η is then, for instance, used to optimize a printed magnet for a portable nuclear magnetic resonance (NMR) device [1]. Although η is an excellent parameter to quantify the overall quality of a homogeneous field, it contains insufficient information for its efficient optimization.

In the context of the mentioned optimization of the magnetic B-field for NMR applications, a typical shimming approach is to compute a series expansion based on spherical harmonics to describe the relevant field component and to improve its homogeneity. For low order terms of this series expansion, a representation based on Cartesian coordinates

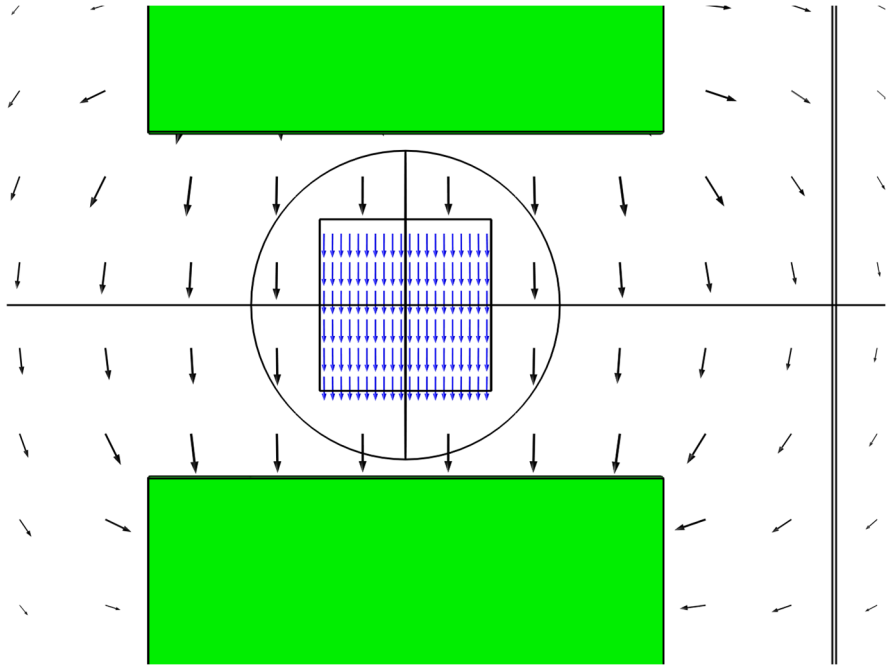

Figure 1: B-field in the air gap of a magnet with a relatively homogeneous field in the ROI (blue arrows); also a detail of the later discussed numerical example in Fig. 10.

helps to understand the vector field and to find a suitable shimming approach [2], [3]. In Noguchi [4] spherical coordinates and real-valued spherical harmonics have been applied, which provide a more concise notation, especially for higher-order terms.

Here, we extend this approach known from NMR magnet shimming with techniques from the boundary element method (BEM) [5]. In the context of the BEM, spherical harmonics and their systematic application are the basis for the fast multipole method (FMM) [6]. Since the studied vector field in the ROI is, in most cases, divergence- and curl-free, it can be represented using the so-called local expansion of its corresponding scalar potential u. Based on Dirichlet and Neumann boundary values on a closed surface surrounding the ROI, the coefficients of the local expansion can be computed robustly and efficiently. A systematic analysis of these coefficients then enables a precise characterization of the vector field and, in the next step, an efficient optimization of the field.

In the following, we first study the local coefficients using a complex-valued representation of spherical harmonics for a more concise notation and show their relation to the distribution of the vector field based on the findings in Buchau [7]. Additional post-processing demonstrates clearly that the local expansion with its local coefficients is a suitable method to characterize vector fields both with a small number of parameters and detailed information about the field, including preservation of properties such as divergence- and curl-freeness. We also discuss the influence of rotations of the coordinate system on the spectrum of local coefficients. In the second part, we show how this introduced systematic field characterization approach can be included in numerical field simulations. To achieve high accuracy and independence of the mesh, direct integration of the field characterization based on a coupling of the finite element method (FEM) and the BEM is preferred [8].

Finally, we give an outlook on how the presented systematic field characterization approach applies to an improved optimization of the distribution of vector fields.

2 THE LOCAL EXPANSION AND ITS COEFFICIENTS

The characteristics of a vector field $\boldsymbol{V}$, e.g. the homogeneity of the magnetic B-field $\boldsymbol{B}$ in NMR applications, are often studied in an ROI, in which $\boldsymbol{V}$ is divergence-free

$$\nabla \cdot \boldsymbol{V} = 0, \tag{2}$$

and curl-free

$$\nabla \times \boldsymbol{V} = \boldsymbol{0}. \tag{3}$$

Then, $\boldsymbol{V}$ can be described based on a scalar potential u

$$\boldsymbol{V} = -\nabla u, \tag{4}$$

which fulfills in the case of homogeneous material properties Laplace's equation

$$\Delta u = 0. \tag{5}$$

Its related Green function for three-dimensional open space field problems is

$$G(\boldsymbol{r}, \boldsymbol{r}') = \frac{1}{4\pi}\frac{1}{|\boldsymbol{r}-\boldsymbol{r}'|}. \tag{6}$$

The point $\boldsymbol{r}'$ is a point on the surrounding boundary elements or the single-layer sources, respectively. The field values are computed at the evaluation point $\boldsymbol{r}$.

The potential in the ROI is obtained from the Dirichlet and Neumann boundary values $u(\boldsymbol{r}')$ and $\frac{\partial u(\boldsymbol{r}')}{\partial n'}$ on the closed surface $\partial\Omega_{\mathrm{ROI}}$ which encloses the domain of the ROI Ω_{ROI}

$$u(\boldsymbol{r}) = \oint_{\partial\Omega_{\mathrm{ROI}}} \left(\frac{\partial u(\boldsymbol{r}')}{\partial n'} G(\boldsymbol{r}, \boldsymbol{r}') - u(\boldsymbol{r}') \frac{\partial G(\boldsymbol{r},\boldsymbol{r}')}{\partial n'} \right) \mathrm{d}A'. \tag{7}$$

Applying eqn (4) on eqn (7) gives

$$\boldsymbol{V}(\boldsymbol{r}) = -\oint_{\partial\Omega_{\mathrm{ROI}}} \left(\frac{\partial u(\boldsymbol{r}')}{\partial n'} \nabla_{\boldsymbol{r}} G(\boldsymbol{r}, \boldsymbol{r}') - u(\boldsymbol{r}') \nabla_{\boldsymbol{r}} \frac{\partial G(\boldsymbol{r},\boldsymbol{r}')}{\partial n'} \right) \mathrm{d}A'. \tag{8}$$

Green's function eqn (6) can be replaced by the truncated series expansion

$$\frac{1}{4\pi}\frac{1}{|\boldsymbol{r}-\boldsymbol{r}'|} = \begin{cases} \frac{1}{4\pi}\sum_{n=0}^{L}\sum_{m=-n}^{n} \frac{r^n}{r'^{n+1}} Y_n^m(\theta,\phi) Y_n^{-m}(\theta',\phi') & r < r' \\ \frac{1}{4\pi}\sum_{n=0}^{L}\sum_{m=-n}^{n} \frac{r'^n}{r^{n+1}} Y_n^m(\theta,\phi) Y_n^{-m}(\theta',\phi') & r' < r, \end{cases} \tag{9}$$

into normalized spherical harmonics

$$Y_n^m(\theta,\phi) = \sqrt{\frac{(n-|m|)!}{(n+|m|)!}} P_n^{|m|}(\cos\theta) \mathrm{e}^{\mathrm{j}m\phi}, \tag{10}$$

where r, θ and ϕ are the spherical coordinates of $\boldsymbol{r}$ and r', θ' and ϕ' are the spherical coordinates of $\boldsymbol{r}'$, respectively. Note, that the imaginary part of the double sum in eqn (9) vanishes. L is the adjustable order of these series expansions.

We define the origin of the used spherical coordinate system in the center of the ROI. Then, we get for the single-layer potential term of eqn (7)

$$u_{sl} = \oint_{\partial\Omega_{\mathrm{ROI}}} \frac{\partial u(\boldsymbol{r}')}{\partial n'} G(\boldsymbol{r}, \boldsymbol{r}') \mathrm{d}A', \tag{11}$$

the corresponding local expansion

$$u_{sl} = \frac{1}{4\pi}\sum_{n=0}^{L}\sum_{m=-n}^{n} r^n Y_n^m(\theta,\phi)\ {}_{sl}L_n^m, \tag{12}$$

with the local coefficients

$${}_{sl}L_n^m = \oint_{\partial\Omega_{\mathrm{ROI}}} \frac{\partial u(\boldsymbol{r}')}{\partial n'} \frac{Y_n^{-m}(\theta',\phi')}{r'^{n+1}}\,\mathrm{d}A'. \tag{13}$$

The part of the double-layer potential of eqn (7)

$$u_{dl} = -\oint_{\partial\Omega_{\mathrm{ROI}}} u(\boldsymbol{r}') \frac{\partial G(\boldsymbol{r},\boldsymbol{r}')}{\partial n'}\,\mathrm{d}A'. \tag{14}$$

Results in a local expansion similar to the one in eqn (12)

$$u_{dl} = \frac{1}{4\pi}\sum_{n=0}^{L}\sum_{m=-n}^{n} r^n Y_n^m(\theta,\phi)\,{}_{dl}L_n^m, \tag{15}$$

since the gradient of Green's function is only applied to the source related term

$${}_{dl}L_n^m = -\oint_{\partial\Omega_{\mathrm{ROI}}} u(\boldsymbol{r}')\boldsymbol{n}'\cdot\nabla_{\boldsymbol{r}'}\frac{Y_n^{-m}(\theta',\phi')}{r'^{n+1}}\,\mathrm{d}A'. \tag{16}$$

The total potential in the ROI is assembled using both eqns (11) and (14)

$$u = u_{sl} + u_{dl}. \tag{17}$$

This means for the corresponding local expansion

$$u = \frac{1}{4\pi}\sum_{n=0}^{L}\sum_{m=-n}^{n} r^n Y_n^m(\theta,\phi) L_n^m, \tag{18}$$

that the local coefficients of both the single-layer and the double-layer terms are added

$$L_n^m = {}_{sl}L_n^m + {}_{dl}L_n^m. \tag{19}$$

Based on the result eqn (19), we can study the properties of the local expansion and its coefficients independent of the applied BEM formulation, indirect formulation based on single-layer sources or direct formulation based on Green's theorem eqn (7). That means the discussion and the results are valid both for indirect and direct BEM formulations.

Although the potential u is a very powerful tool to simply describe the studied vector field $\boldsymbol{V}$ using the local expansion eqn (18), we need additionally the relation between the local coefficients eqn (19) and $\boldsymbol{V}$. To apply eqn (4) on eqn (18), we have two options. The gradient in eqn (4) has to be evaluated in Cartesian coordinates in arbitrary points in the ROI. To evaluate the gradient easily, the local expansion can be converted into a series expansion using spherical harmonics in Cartesian coordinates first [2]. For low-order terms, this approach is helpful and typically used for shimming magnets. However, we prefer here a notation, which is applicable in general including higher-order terms. Hence, we use the more concise notation of spherical harmonics based on spherical coordinates and complex values. Since the spherical coordinates are not defined in the origin of the coordinate system, which lies in the center of the ROI, and in the poles, we have to evaluate the limits approaching these points. Fortunately, both u and $\boldsymbol{V}$ are continuous in the complete ROI. Computing the limits defines the directions of the basis vectors in spherical coordinates, too. Applying the gradient eqn (4) to eqn (18) means that the gradient of the spherical harmonics is required

$$\boldsymbol{V} = -\frac{1}{4\pi}\sum_{n=1}^{L}\sum_{m=-n}^{n} \nabla\big(r^n Y_n^m(\theta,\phi)\big) L_n^m. \tag{20}$$

Note, that the potential is constant for $n = 0$. As shown in Buchau et al. [9], the derived vector field in the origin of the coordinate system or the center of the ROI respectively is

$$\boldsymbol{V} = -\frac{1}{4\pi}\begin{pmatrix} -\sqrt{2}\Re\{L_1^1\} \\ \mathrm{j}\sqrt{2}\Im\{L_1^1\} \\ L_1^0 \end{pmatrix}, \tag{21}$$

in the poles ($\theta = 0$ or $\theta = \pi$)

$$\boldsymbol{V} = -\frac{1}{4\pi}\begin{pmatrix} \frac{1}{z}\sum_{n=1}^{L} r^n \left(\frac{\partial P_n^0(\cos\theta)}{\partial\theta} L_n^0 + 2\sum_{m=1}^{n} \sqrt{\frac{(n-m)!}{(n+m)!}} \frac{\partial P_n^m(\cos\theta)}{\partial\theta} \Re\{L_n^m\} \right) \\ \frac{1}{z}\sum_{n=1}^{L} r^n \left(\frac{\partial P_n^0(\cos\theta)}{\partial\theta} L_n^0 + 2\sum_{m=1}^{n} \sqrt{\frac{(n-m)!}{(n+m)!}} \frac{\partial P_n^m(\cos\theta)}{\partial\theta} \Re\left\{ \mathrm{e}^{\mathrm{j}m\frac{\pi}{2}} L_n^m \right\} \right) \\ \sum_{n=1}^{L} nzr^{n-2} (Y_n^0(\theta,\phi) L_n^0 + 2\sum_{m=1}^{n} \Re\{Y_n^m(\theta,\phi) L_n^m\}) \end{pmatrix}, \tag{22}$$

and in all the other points

$$\boldsymbol{V} = \frac{-1}{4\pi}\sum_{n=1}^{L}\sum_{m=-n}^{n} L_n^m \begin{pmatrix} Y_n^m \left(nxr^{n-2} - \frac{\mathrm{j}myr^n}{x^2+y^2} \right) + \sqrt{\frac{(n-|m|)!}{(n+|m|)!}} \frac{\partial P_n^{|m|}}{\partial\theta} \frac{xzr^{n-2}}{\sqrt{x^2+y^2}} \mathrm{e}^{\mathrm{j}m\phi} \\ Y_n^m \left(nyr^{n-2} + \frac{\mathrm{j}mxr^n}{x^2+y^2} \right) + \sqrt{\frac{(n-|m|)!}{(n+|m|)!}} \frac{\partial P_n^{|m|}}{\partial\theta} \frac{yzr^{n-2}}{\sqrt{x^2+y^2}} \mathrm{e}^{\mathrm{j}m\phi} \\ Y_n^m nzr^{n-2} - \sqrt{\frac{(n-|m|)!}{(n+|m|)!}} \frac{\partial P_n^{|m|}}{\partial\theta} \sqrt{x^2+y^2} r^{n-2} \mathrm{e}^{\mathrm{j}m\phi} \end{pmatrix}. \tag{23}$$

To keep the computational costs as small as possible, only the real part of eqn (23) is evaluated in practice. Then, it is sufficient to start the inner summation for $m = 0$.

The gradient of spherical harmonics in eqn (16) doesn't require different cases and is

$$\nabla_{\boldsymbol{r}} \frac{Y_n^m(\theta,\phi)}{r^{n+1}} = \begin{pmatrix} -(n+1)\frac{x}{r^{n+3}} Y_n^m(\theta,\phi) + \frac{1}{r^{n+1}} \frac{\partial}{\partial x} Y_n^m(\theta,\phi) \\ -(n+1)\frac{y}{r^{n+3}} Y_n^m(\theta,\phi) + \frac{1}{r^{n+1}} \frac{\partial}{\partial y} Y_n^m(\theta,\phi) \\ -(n+1)\frac{z}{r^{n+3}} Y_n^m(\theta,\phi) + \frac{1}{r^{n+1}} \frac{\partial}{\partial z} Y_n^m(\theta,\phi) \end{pmatrix}, \tag{24}$$

with

$$\frac{\partial}{\partial x} Y_n^m(\theta,\phi) = \sqrt{\frac{(n-|m|)!}{(n+|m|)!}} \left(-\frac{\mathrm{j}m\mathrm{e}^{\mathrm{j}m\phi} y}{x^2+y^2} P_n^{|m|}(\cos\theta) + \frac{\mathrm{e}^{\mathrm{j}m\phi} xz}{r^2\sqrt{x^2+y^2}} \frac{\partial P_n^{|m|}(\cos\theta)}{\partial\theta} \right), \tag{25}$$

$$\frac{\partial}{\partial y} Y_n^m(\theta,\phi) = \sqrt{\frac{(n-|m|)!}{(n+|m|)!}} \left(\frac{\mathrm{j}m\mathrm{e}^{\mathrm{j}m\phi} x}{x^2+y^2} P_n^{|m|}(\cos\theta) + \frac{\mathrm{e}^{\mathrm{j}m\phi} yz}{r^2\sqrt{x^2+y^2}} \frac{\partial P_n^{|m|}(\cos\theta)}{\partial\theta} \right), \tag{26}$$

and

$$\frac{\partial}{\partial z} Y_n^m(\theta,\phi) = \sqrt{\frac{(n-|m|)!}{(n+|m|)!}} \left(-\frac{\sqrt{x^2+y^2}}{r^2} \mathrm{e}^{\mathrm{j}m\phi} \frac{\partial P_n^{|m|}(\cos\theta)}{\partial\theta} \right). \tag{27}$$

2.1 Local coefficients and their impact on the vector field

In the first part of our study about local coefficients, we investigated the impact of the local coefficients both on the potential u and the corresponding vector field $\boldsymbol{V}$.

We set the considered real or imaginary part to the value 1.0 and all other coefficients to zero. Then we evaluated the local expansion for the potential eqn (18) and its gradient eqns

(21)–(23) on a regular grid from –1.0 m to 1.0 m in all three directions of the Cartesian coordinate system. The center of the local expansion was set to the origin of this coordinate system. The potential is visualized with the help of isosurfaces. Arrows with lengths proportional to the norm of the vector field in the grid points are used for the corresponding vector field visualization. Both fields are plotted dimensionless.

The test environment is implemented in our in-house code MuPhyN in C#, which also contains the implementation of the FMM and BEM of Buchau [8], and in MATLAB to provide a tool that can be applied automatically for arbitrary order of the series expansions.

There is only one local coefficient for $n = 0$. It results in a constant potential within the complete ROI

$$u_{n=0} = \frac{1}{4\pi} r^0 Y_0^0(\theta, \phi) L_0^0 = \frac{1}{4\pi} L_0^0, \tag{28}$$

along with a vanishing vector field $\boldsymbol{V} = \boldsymbol{0}$. That means, the coefficient L_0^0 sets a constant potential in the ROI and does not influence the vector field itself.

For $n = 1$, three parts of the local coefficients are relevant. The terms of $m = 0$ have a real part only. The real part of the local coefficient L_1^0 sets the linear term of the potential u in z-direction and is independent of the x- and y-coordinates (Fig. 2). Evaluating eqn (23) gives the constant vector field component V_z (Fig. 2). The real part of L_1^1 controls the linear term of the potential u in x-direction along with the constant component V_x of the vector field (Fig. 3) and the imaginary part of L_1^1 gives the linear term of the potential u in y-direction along with the constant component V_y of the vector field (Fig. 4).

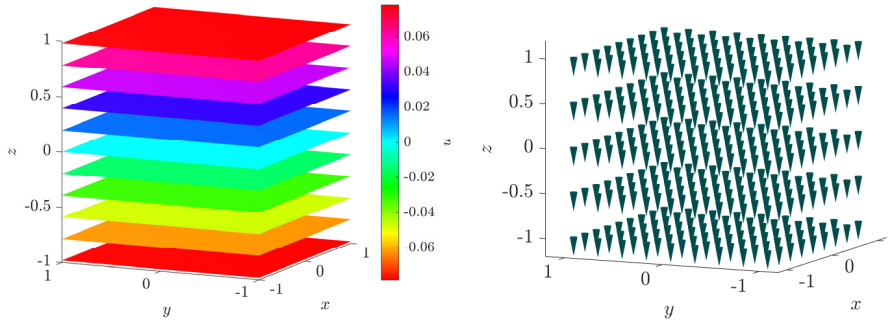

Figure 2: The potential (left) and the vector field (right) in dependency of $\Re\{L_1^0\}$.

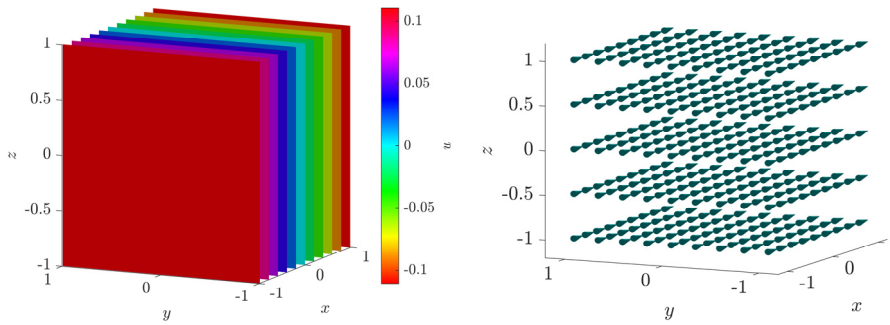

Figure 3: The potential (left) and the vector field (right) in dependency of $\Re\{L_1^1\}$.

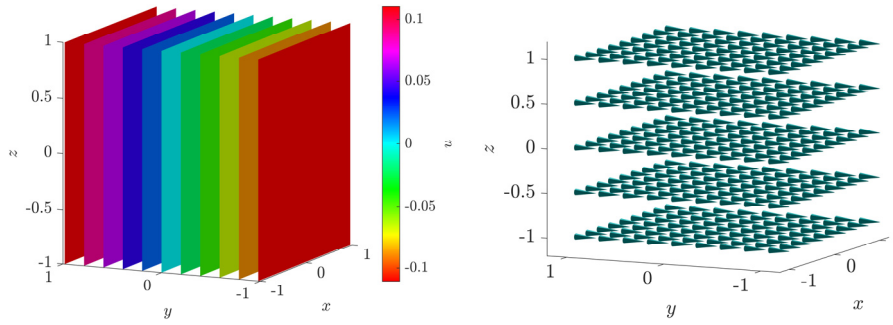

Figure 4: The potential (left) and the vector field (right) in dependency of $\Im\{L_1^1\}$.

The quadratic terms of u and the linear terms of $\boldsymbol{V}$ are exemplarily shown in Fig. 5 for the real part of L_2^0 and in Fig. 6 for the imaginary part of L_2^1. The properties of a vector field with a linear dependency on the y-coordinate of its z-component in the xy-plane are clearly visible in Fig. 6. Note, the plotted field term has not only the mentioned linear dependency on the y-coordinate in the xy-plane but additionally provides a field distribution of a divergence- and curl-free vector field. This information is very important for the topology and shape optimization of the studied device.

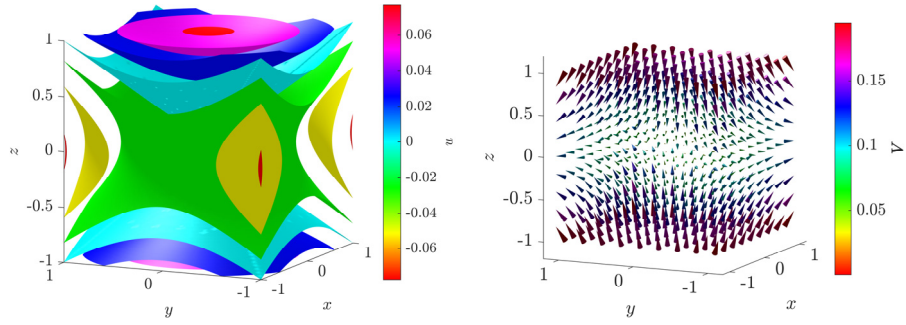

Figure 5: The potential (left) and the vector field (right) in dependency of $\Re\{L_2^0\}$.

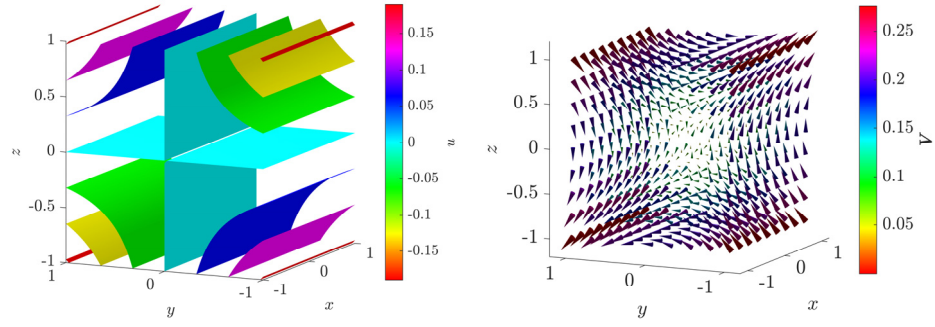

Figure 6: The potential (left) and the vector field (right) in dependency of $\Im\{L_2^1\}$.

We visualized in Fig. 7 one of the quintic terms of the potential and its corresponding quartic term of the vector field to show that our study applies to arbitrary order of the local expansion and provides a catalog of field terms based on the local expansion.

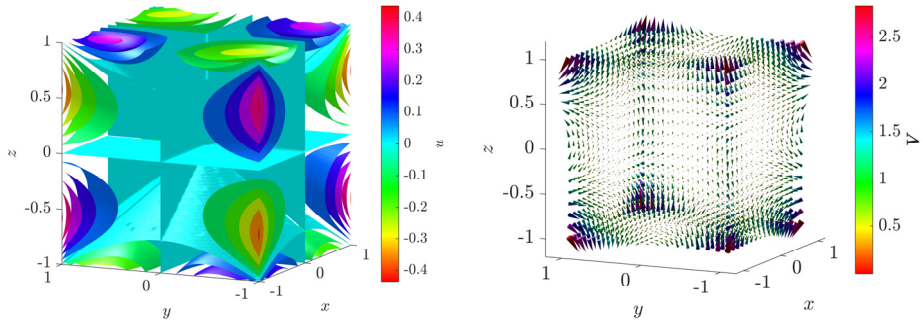

Figure 7: The potential (left) and the vector field (right) in dependency of $\Im\{L_5^2\}$.

Furthermore, the discussed terms show that the field in the ROI is influenced differently. With increasing order, the field is shaped for a larger distance to the center of the ROI.

2.2 Rotation of the coordinate system

Before we use the catalog of the previous subsection for a systematic analysis of a field, we discuss here the influence of a rotation of the coordinate system. A rotation of the coordinate system represents the typical situation where the coordinate system is not moved but a misalignment of the plane, in which the field is measured or evaluated, is taken into account.

Rotations of the coordinate system and their effect on the local coefficients are discussed for instance in Greengard and Rokhlin [10] in detail. There, the rotations of already computed local coefficients are considered as a part of the translation operators within the algorithm of the FMM. Here, we revisit the rotations and discuss them in the context of the proposed field characterization.

First, we study the effect of a rotation of the coordinate system around the z-axis by the angle β. That means, the spherical coordinates r, θ and ϕ are transformed into r, θ and ϕ' with the new local coefficients

$$L'^{m}_{n} = R_z(m,\beta)L^{m}_{n}, \tag{29}$$

where

$$R_z(m,\beta) = \mathrm{e}^{\mathrm{j}m\beta}. \tag{30}$$

Are the rotation coefficients. It can be seen that both the degree n and the order m are left unchanged during the rotation around the z-axis. The transformation eqn (29) changes the phase of the complex coefficient and along with the findings in the previous subsection the dependency of the computed field on the x- and y-coordinates.

A rotation around the y-axis by the angle α transforms the spherical coordinates r, θ and ϕ into r, θ' and ϕ'. The related transformation is

$$L'^{m'}_{n} = \sum_{m=-n}^{n} R_y(n,m,m',\alpha)L^{m}_{n}, \tag{31}$$

With the rotation coefficients $R_y(n, m, m', \alpha)$, which can be found in Greengard and Rokhlin [10]. They contain powers of the trigonometric functions and Jacobi polynomials that can be computed recursively.

The rotation about the y-axis preserves the degree n of the local coefficients but not the order m. Again, the coordinate dependency is influenced by this rotation.

3 ANALYSIS OF SIMULATED FIELDS

Here, we suggest a generally applicable approach to characterize vector fields inside the ROI based on numerical field computations using the finite element method (FEM), the boundary element method (BEM), or a combination of the two, as discussed in Buchau [8].

In the first step, the domain Ω_{ROI} of the ROI has to be defined. A requirement for our approach is that the studied vector field $\boldsymbol{V}$ must be divergence- and source-free in the ROI and that the material properties are linear, homogeneous, and isotropic. Often, the domain Ω_{ROI} is filled with air, and these requirements are fulfilled.

The closed surface of Ω_{ROI} is $\partial\Omega_{\mathrm{ROI}}$. Since the local coefficients are here computed directly by integrals over $\partial\Omega_{\mathrm{ROI}}$ in eqns (13) and (16), it must be ensured that the smallest distance of any boundary element on $\partial\Omega_{\mathrm{ROI}}$ is larger than the radius of the sphere, which encloses the ROI. Otherwise, the strict separation of the evaluation point and the source point in eqn (9) is violated. In practice, we prefer a domain Ω_{ROI}, which is as large as possible but not intersecting neighbor domains. Furthermore, a small gap to adjacent material domains increases the numerical accuracy [8]. A typical situation is depicted in Fig. 8 for a magnet design of an NMR application. There, the non-linear magnetic field problem is typically solved using the FEM. Then, the BEM, along with the local expansion, is applied in Ω_{ROI}, which is only a small part of the air gap between the pole shoes of the yoke and enclosing the ROI.

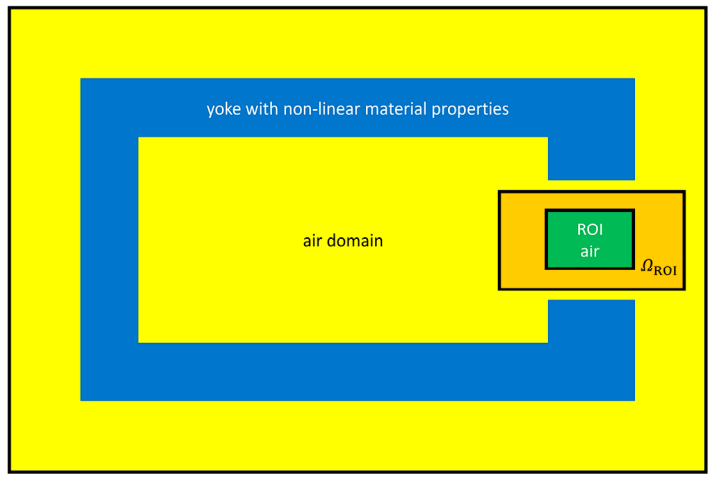

Figure 8: Definition of Ω_{ROI} and $\partial\Omega_{\mathrm{ROI}}$ for a magnet.

For an evaluation of eqn (7), the Dirichlet and Neumann values $u(\boldsymbol{r}')$ and $\frac{\partial u(\boldsymbol{r}')}{\partial n'}$ of the potential u at the boundary $\partial\Omega_{\mathrm{ROI}}$ are required. Whilst $\frac{\partial u(\boldsymbol{r}')}{\partial n'}$ is related to the normal

component of the vector field $\boldsymbol{V}$ and accessible in the numerical field computation, $u(\boldsymbol{r}')$ is not directly available in typical numerical formulations. In most cases, $\boldsymbol{V}$ is not curl-free, and a formulation based on the vector field itself or a vector potential is applied.

The closed surface $\partial\Omega_{\mathrm{ROI}}$ is classically discretized using nodal elements with Lagrange polynomials of second-order as shape and ansatz functions. There are several ways to obtain the boundary values, which we discuss here. After determining the nodal values of the Dirichlet and Neumann boundary values, the local coefficients are directly computed by an evaluation of eqns (13) and (16). Depending on the demands for the vector field characterization, highly accurate boundary values along with a carefully selected number of Gaussian points for the numerical integration are needed.

The most generally applicable approach is to solve the field problem completely independent of the field characterization step, e.g. using the FEM. In some cases, the scalar potential of the FEM solution along with the corresponding flux values at the position of the nodes of the boundary elements for the field characterization is directly computed. The accuracy of these values depends strongly on the quality of the mesh close to $\partial\Omega_{\mathrm{ROI}}$. An improvement would be to mesh $\partial\Omega_{\mathrm{ROI}}$ in the FEM model, too. Then, it is easier to control the mesh size and quality, but smoothing techniques are required to tackle the problem of only C^0-continuity of the Lagrange elements. If the FEM simulation can be directly coupled with the field characterization, the boundary values can be computed at the Gaussian points of the integrals in eqns (13) and (16), and discontinuities of the flux in the element nodes are not relevant. These values are also used in cases where another formulation than the one based on a scalar potential is applied. Since in this case the scalar potential is unknown, it must be computed with another BEM-based step. That means, after the solution of the field problem using the FEM, a BEM problem with the flux values from the FEM is solved to compute the potential values.

We prefer a solution of the field problem based on a coupling of the FEM and the BEM as suggested e.g. in [8]. The domain Ω_{ROI} is solved with the BEM and the remaining domain with the FEM, or in general, with an arbitrary numerical method. The required Dirichlet and Neumann boundary values are obtained with high accuracy since the continuity conditions are evaluated in the Gaussian points of the related Galerkin integrals, where the Lagrange elements are always smooth. Such a coupling is even possible in cases with a vector potential or vector field formulation in the remaining domain. The boundary values computed in this way are then used to derive the local coefficients.

We implemented the proposed approach using the commercial software COMSOL Multiphysics for the field computation, our in-house code MuPhyN and MATLAB as interface. The shown example (Fig. 9) uses a scalar potential formulation to solve the non-linear magnetic field problem both for the FEM and the BEM domain Ω_{ROI}. The permanent magnet has a remanence flux density of 1.2 T. The yoke is made of soft iron, and its material properties are modeled using a non-linear BH-curve. The FEM domain is discretized using 1,512,290 second-order tetrahedrons and the BEM surface with 238 second-order triangles. In total, a non-linear equation system with 2,022,453 unknowns was solved using a Newton–Raphson method and GMRES with a direct preconditioner on an Intel Xeon E3-1275 v5 with a clock speed of 3.60 GHz and DDR4 RAM at 2,133 MHz in 385 seconds. The matrix of the BEM was compressed using the adaptive cross approximation technique (ACA). The B-field of the complete configuration is shown in Fig. 10 and in the ROI in Fig. 1.

Although the B-field in the ROI appears homogeneous (Fig. 1), its homogeneity value is only $\eta = 14\%$. In general, a quantitative comparison to a perfectly homogeneous field is missing in the field plot.

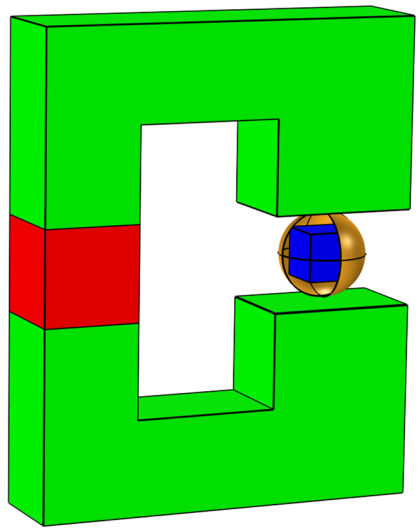

Figure 9: Magnetic circuit with non-linear iron yoke (green), permanent magnet (red), ROI (blue) and Ω_{ROI} (orange).

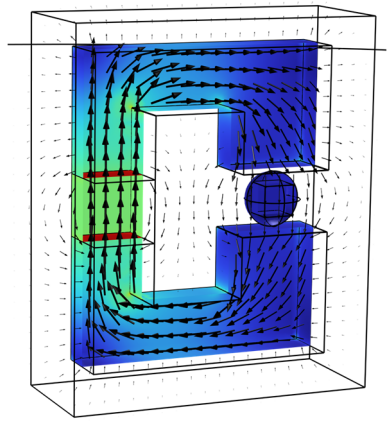

Figure 10: B-field of the magnet obtained using the FEM coupled with the BEM.

We tested our proposed new field characterization approach using this example. Therefore, we imported the solution of the BEM, including the boundary element mesh via the MATLAB interface from COMSOL Multiphysics to our in-house code MuPhyN. Finally, we obtained the corresponding set of local coefficients, which describe the scalar magnetic potential and the B-field in the ROI.

As can be seen from eqn (9), the distances to the origin always occur in the combination $\frac{r^n}{r'^{n+1}}$ or $\frac{r'^n}{r^{n+1}}$. To avoid a misinterpretation of the spectrum of local coefficients, we normalized the local coefficients obtained from eqns (13) and (16) by multiplying them with the factor r^n. For r, we selected the maximum distance of points in the ROI to its center.

Then, the values are better comparable. The normalized local coefficient spectrum is depicted in Fig. 11.

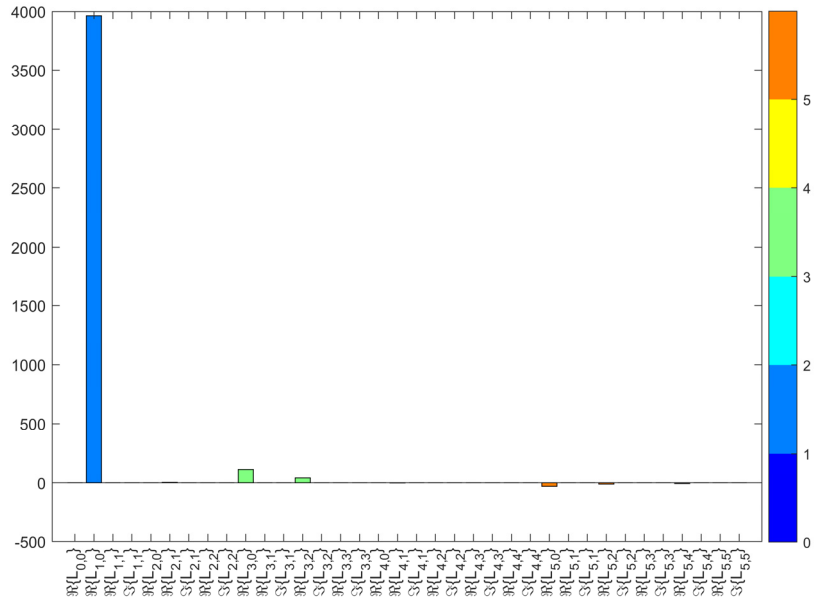

Figure 11: The spectrum of normalized local coefficients of the magnet.

4 COMBINATION WITH OPTIMIZATION AND MACHINE LEARNING

The normalized spectrum of local coefficients in the previous section (Fig. 11) clearly shows that one linear term for the potential is dominant but some 3rd- and 5th-order terms are relevant, too. Comparing the spectrum with the plots of the local coefficients gives additional information about the vector field distribution related to the coefficient. A goal of the following optimization of the magnet could be now to minimize the unwanted non-zero terms in the spectrum without creating new terms by an appropriate shimming and design optimization. For arbitrary field distributions, the reference spectrum has to be calculated first.

We see large potential for using our field characterization approach in the context of optimization and machine learning. First, the spectrum of local coefficients shows directly in which way the field inside the complete ROI differs from the reference field distribution, and suggestions for improving the design can be made based on experience and databases. Second, the values of the coefficients in combination with weighting factors can be used as the cost function for optimization algorithms. Finally, the presented spectrum is very well suited for deep learning approaches as the input parameters instead of the field itself.

5 CONCLUSIONS

We presented a very powerful approach to characterize vector fields accurately but with only a small set of coefficients. Our approach based on the local expansion, which is well-known from the FMM, combines techniques of different disciplines to provide a generally applicable tool for optimizing vector fields. It can be used both with commercial field solvers and research implementations of numerical methods. The computed spectrum of local

coefficients is highly accurate and contains important information about the studied vector field with only a few parameters. Hence, this approach is very well suited not only for the characterization of a vector field but also for optimization using the spectrum as the cost function.

REFERENCES

[1] Alnajjar, B., Buchau, A., Baumgärter, L. & Anders, J., NMR magnets for portable applications using 3D printed materials. *Journal of Magnetic Resonance,* **326**, 2021. DOI: 10.1016/j.jmr.2021.106934.

[2] Anderson, W.A., Electrical current shims for correcting magnetic fields. *Review of Scientific Instruments,* **32**(3), pp. 241–250, 1961. DOI: 10.1063/1.1717338.

[3] Williams, J.E.C., Superconducting magnets for MRI. *IEEE Transactions on Nuclear Science,* **31**(4), pp. 994–1005, 1984. DOI: 10.1109/TNS.1984.4333424.

[4] Noguchi, S., Formulation of the spherical harmonic coefficients of the entire magnetic field components generated by magnetic moment and current for shimming. *Journal of Applied Physics,* **115**, 2014. DOI: 10.1063/1.4872244.

[5] Brebbia, C.A., Telles, J.C.F. & Wrobel, L.C., *Boundary Element Techniques*, Springer-Verlag: Berlin and New York, 1984.

[6] Greengard, L. & Rokhlin, V., The rapid evaluation of potential fields in three dimensions. *Vortex Methods. Lecture Notes in Mathematics*, vol. 1360, eds C. Anderson & C. Greengard, Springer, 1988. DOI: 10.1007/BFb0089775.

[7] Buchau, A., Accuracy analysis of the fast multipole method for three-dimensional boundary value problems based on Laplace's equation. *WIT Transactions on Engineering Sciences*, vol. 131, WIT Press: Southampton and Boston, pp. 3–15, 2021. DOI: 10.2495/BE440011.

[8] Buchau, A., Precise and robust magnetic field computations for high-end smart sensor applications. *WIT Transactions on Engineering Sciences*, vol. 126, WIT Press: Southampton and Boston, pp. 75–87, 2019. DOI: 10.2495/BE420071.

[9] Buchau, A., Huber, C.J., Rieger, W. & Rucker, W.M., Fast BEM computations with the adaptive multilevel fast multipole method. *IEEE Transactions on Magnetics*, **36**(4), pp. 680–684, 2000. DOI: 10.1109/20.877540.

[10] Greengard, L. & Rokhlin, V., A new version of the fast multipole method for the Laplace equation in three dimensions. *Acta Numerica,* **6**, pp. 229–269, 1997. DOI: 10.1017/S0962492900002725.